JACS
JOURNAL OF THE AMERICAN CHEMICAL SOCIETY
Article
Cite This: J. Am. Chem. Soc. 2018, 140, 1824−1833
pubs.acs.org/JACS

Hydrophobic CuO Nanosheets Functionalized with Organic Adsorbates

Yulian He,[†] Zachary S. Fishman,[†] Ke R. Yang,[‡,§] Brandon Ortiz,[†] Chaolun Liu,[∥] Julia Goldsamt,[⊥] Victor S. Batista,*[,‡,§] and Lisa D. Pfefferle*[,†]

[†]Department of Chemical & Environmental Engineering, Yale University, New Haven, Connecticut 06520-8286, United States
[‡]Department of Chemistry, Yale University, New Haven, Connecticut 06520-8107, United States
[§]Energy Science Institute, Yale University, West Haven, Connecticut 06516-7394, United States
[∥]Department of Chemistry, University of Hawaii at Manoa, Honolulu, Hawaii 96816, United States
[⊥]Great Neck North High School, Great Neck, New York 11023, United States

Supporting Information

ABSTRACT: A new class of hydrophobic CuO nanosheets is introduced by functionalization of the cupric oxide surface with *p*-xylene, toluene, hexane, methylcyclohexane, and chlorobenzene. The resulting nanosheets exhibit a wide range of contact angles from 146° (*p*-xylene) to 27° (chlorobenzene) due to significant changes in surface composition induced by functionalization, as revealed by XPS and ATR-FTIR spectroscopies and computational modeling. Aromatic adsorbates are stable even up to 250−350 °C since they covalently bind to the surface as alkoxides, upon reaction with the surface as shown by DFT calculations and FTIR and ^{1}H NMR spectroscopy. The resulting hydrophobicity correlates with H_2 temperature-programmed reduction (H_2-TPR) stability, which therefore provides a practical gauge of hydrophobicity.

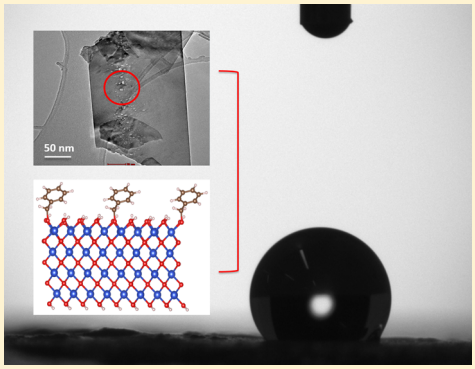

INTRODUCTION

Nanomaterials offer a versatile framework for engineering surfaces with specific functionalities,[1,2] as required for applications with constraints on the chemical, mechanical, magnetic, electronic and optical properties of the materials. Traditionally, properties of nanomaterial surfaces have been tuned by doping[3−5] or by controlling the nanoparticle size,[6−9] shape,[7,10,11] dimension, and chirality.[1] Functionalization based on covalent binding of adsorbates to the material surface is becoming an increasingly popular strategy for tuning the properties of nanomaterials.[4,12] Compared to dopants that are often integrated into the lattice, functional groups are only chemically bonded to the surface. Nevertheless, they can dramatically affect the properties of the materials,[4] particularly for nanosheets where a large fraction of the atoms are surface exposed. Here, we focus on functionalization of metal oxide surfaces with hydrophobic adsorbates such as CuO nanosheets functionalized with *p*-xylene, toluene, hexane, methylcyclohexane (MCH), and chlorobenzene (CB).

Many studies have focused on functionalizing carbonaceous systems such as carbon nanotubes[13−21] and graphenes[4,22−26] with oxygen, nitrogen, sulfur, boron, and other moieties to drastically change their properties. For instance, carbon nanotubes functionalized with sulfur groups showed increased mechanical strength due to denser packing.[27] Functionalization of gold and silver nanoparticles typically involves thiol and amine groups.[2,28,29] Nanowires have been functionalized with biologically relevant molecules for sensing or drug delivery.[30] Surfactants and polymers have been employed as capping agents to enhance dispersibility and antimicrobial activity.[31,32]

Functionalization of metal oxides in particular is gaining increasing attention owing to their dynamic properties and extensive use in electronics,[33] catalysis,[34] and other applications. Silicon polymers have been explored to functionalize copper oxide and other metal oxides to increase hydrophobicity and photocatalytic activity.[35−37] Superhydrophobic CuO is reported to be more corrosion-resistant, suggesting that reactions involving water may be controlled using functionalization.[38] Though much has been done toward functionalizing metal oxides for superhydrophobicity, most of them involve the use of fluorinated compounds, which are highly toxic and environmental hazardous.[39] Still, large classes of molecules and materials remain unexplored, or poorly understood. Rigorous characterization and theoretical studies are needed to establish the nature of these surfaces and the binding modes of molecular adsorbates.

Reactions of small organic/aromatic molecules over inorganic materials have been studied for decades, including numerous reactions over copper oxide catalysts.[40−43] Copper

Received: November 2, 2017
Published: January 3, 2018

DOI: 10.1021/jacs.7b11654
J. Am. Chem. Soc. 2018, 140, 1824−1833

oxide is particularly attractive since it is a nonhazardous material composed of earth abundant elements. For example, mesoporous $CuMnCeO_x$ with different CuO and MnO_x doping contents were shown to catalyze CB decomposition,[41] while copper oxide on mesostructured silica was shown to dehydrogenate cylcohexane.[43] Gaseous toluene was found to be oxidized over metal oxides, including copper oxide.[44] Most of these earlier reports focus on characterization of the reaction itself although in general they do not investigate how the reaction affects the catalytic surface as explored in our study.

Functionalization can be exploited to change the properties of the surfaces in a wide range of possibilities. We focus on hydrophobicity that can enhance stability under aqueous conditions. There is already a growing interest in inorganic hydrophobic materials such as copper oxide.[37,45−49] Current technologies utilize coated or nanopatterned surfaces although they often involve environmentally hazardous materials or are economically demanding.[50] Copper oxides are attractive alternatives offering a valuable framework to investigate how changes in structure and composition affect hydrophobicity.[45,47] Except for a few studies which examined CuO functionalized with silicon polymers,[37,49] functionalization of CuO for hydrophobicity has remained unexplored.

We demonstrate that the hydrophobicity of copper oxide nanosheets may be tuned by functionalizing the surface with small organic molecules such as toluene, *p*-xylene, hexane, MCH, and CB. We use an assortment of characterization tools and computations to show that these organic molecules become strongly bonded to the CuO surface as alkoxides without changing the nanostructure or crystal structure of the material. Experimental work is supported by DFT calculations exploring the binding process at the molecular level. Finally, we demonstrate the stability of these materials in both oxidative and reductive atmospheres.

■ EXPERIMENTAL SECTION

All chemicals used here were purchased from Sigma-Aldrich with purity ≥97%. Gases used were ultrahigh purity (UHP) grade purchased from AirGas.

Functionalization of CuO Nanosheets. CuO nanosheets were synthesized via a soft templating method following the same protocols from our previous work.[51] 200 mg of CuO nanosheets were dispersed in 100 mL of organic solvents, including toluene, *p*-xylene, hexane, MCH, or CB depending on the treatment and refluxed for 24 h. The solution was then filtered, and the precipitate was washed with additional solvent. After the filtration, samples were vacuum-dried in a desiccator for 2 days and finely ground with mortar and pestle before further measurements.

Characterization details on contact angle measurement, scanning electron microscopy, transmission electron microscopy, X-ray diffraction, Fourier transform infrared spectroscopy-ATR, X-ray photoelectron spectroscopy, X-ray fluorescence, proton-nuclear magnetic resonance spectroscopy, thermogravimetric analysis, BET physisorption and H_2 temperature-programmed reduction H_2-TPR are given in the Supporting Information.

Molecular Modeling. DFT calculations with periodic boundary calculations were performed with the Vienna ab initio simulation package (VASP)[52−55] version 5.4.1. The projector augmented plane wave (PAW) method[56,57] together with the PBE exchange-correlation functional[58] were employed to describe the electron−ion interactions. The PBE + U method following Dudarev's approach[59] was implemented to add on-site potentials to the d electrons of transition metals and properly describe the electronic states. $U_{eff} = U - J$ parameter of 7.5 eV was used to reproduce the experimental band gap of bulk metal oxides. A cutoff of 450 eV was chosen for the plane wave basis set and a 7 × 7 × 7 Monckhorst-Pack type k-point grid for bulk geometry optimization. A Gaussian smear was used with a $\sigma = 0.1$ eV. The energy convergence criterion was 10^{-4} eV per unit cell, and the force convergence criterion was defined as 0.01 eV $Å^{-1}$ for geometry optimization. Supercells with dimensions of 9.38 Å × 6.86 Å × 25.26 Å with OH termination were used to model the CuO (002) surface that reproduce the experimentally observed band gap of CuO nanosheets. A 3 × 3 × 1 Monkhorst−Pack k-point mesh was used for all slab calculations. Dispersion interactions are important in the binding of small molecules to CuO surfaces, and they were treated with Grimme's D3 version correction with Becke−Johnson damping function.[60,61] For small adsorbate molecules calculations, a supercell of 20 Å × 20 Å × 20 Å and a 1 × 1 × 1 Monkhorst−Pack k-point mesh was used. The reaction free energy changes were calculated as $\Delta G = \Delta E + \Delta(ZPE) - T\Delta S$, where ΔE, $\Delta(ZPE)$, and ΔS are electronic energy, zero-point energy, and entropy difference between products and reactants. The zero-point energies of isolated and absorbed molecules were calculated from the frequency analysis performed by VASP. The entropies of isolated molecules were calculated with the PBE functional and the 6-31G(d) basis set,[62] as implemented in Gaussian 09 software package (revision E.01).[63] Dispersion effects were again considered by Grimmes' D3 version with Becke-Johnson damping function. The entropies of absorbed species were calculated from the partition function by treating all degrees of freedom as vibrational. The quasiharmonic approximation, with vibrational frequencies lower than 60 cm^{-1} raised to 60 cm^{-1}, was used in the calculation of partition functions to correct the well-known breakdown of the harmonic oscillator model for the entropy of low-frequency vibrational modes.[64] The visualization of structures were performed with *VESTA* software package version 3.[65]

■ RESULTS AND DISCUSSION

Hydrophobicity. Copper oxide nanosheets were synthesized and then functionalized by reflux in various solvents to increase their hydrophobicity. The solvents were selected to test the effects of different molecular structures. Hexane was selected for functionalization with a linear alkane, MCH as a model cyclic hydrocarbon, toluene and *p*-xylene as aromatic rings, and CB was selected to determine the influence of a halo group on the reaction.

Contact angle measurements were performed with water droplets on films rolled from powder functionalized and untreated CuO nanosheets, shown in Figure 1. Untreated CuO nanosheets were found to be hydrophilic, absorbing water and giving no contact angle. All functionalization treatments investigated increased the contact angle of the nanosheets. The most dramatic hydrophobic effects were obtained with toluene and *p*-xylene treatments that increased the contact angle of the CuO nanosheets to 134 and 146°, respectively,

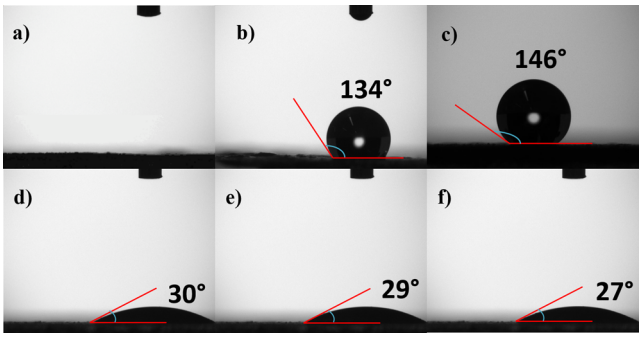

Figure 1. Contact angle measurements of (a) untreated and (b) toluene-treated (134°), (c) *p*-xylene-treated (146°), (d) hexane-treated (30°), (e) MCH-treated (29°), and (f) CB-treated (27°) CuO nanosheets.

DOI: 10.1021/jacs.7b11654
J. Am. Chem. Soc. 2018, 140, 1824−1833

Table S1. Surprisingly, functionalization with CB increased the contact angle by only 27°, comparable to modest contact angles typically produced by functionalization with nonaromatic compounds (e.g., 29° for MCH and 30° for hexane). Clearly, the chemical nature of the aromatic group plays an important role in determining the hydrophobicity of the resulting material. In subsequent sections, we show how methylated benzene rings have the ability to bind to CuO nanosheets and how halo and alcohol groups can limit the binding process.

As a control, CuO nanosheets were immersed into toluene without heating for 24 h. We found no change in the contact angle for this sample, indicating that reflux is essential for functionalization. In addition, commercial bulk CuO was refluxed in toluene and found to be hydrophobic by drop testing in DI water (data not shown).

Nanostructure and Crystal Structure. The hydrophobicity of a surface can increase with changes in nanostructure that increase the surface area and roughness. Jagged and sharp edges increase the hydrophobicity of hydrophobic materials as well as the hydrophilicity of hydrophilic surfaces. Our TEM and SEM analysis of treated and untreated CuO nanosheets, however, determined that our functionalization treatments did not altered the nanostructure (Figures 2 and S1). We found that for all of the surfaces

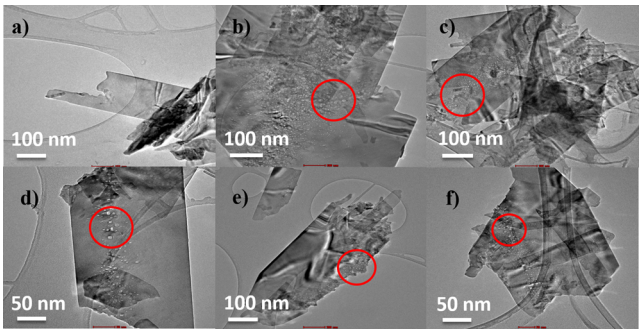

Figure 2. TEM images of (a) untreated and (b) toluene-treated, (c) *p*-xylene-treated, (d) hexane-treated, (e) MCH-treated, and (f) CB-treated CuO nanosheets. The red circles reveal the large defects.

investigated the structure of the nanosheets was largely unperturbed. All materials, functionalized or not, were nanosheets ranging from 250 to 1000 nm in length and width. From AFM in previous work,[51] we know that the nanosheets are 10−20 nm in thickness. Compared to the untreated sample, there are hardly any changes in the sharpness of the edges of the nanosheets. However, from visual inspection of the nanosheets, we see an increase in the number of large defects.

BET (Brunauer, Emmett, and Teller) measurements of the specific surface area, including the pore size distribution, were performed to see if the creation or enlargement of these defects had any impact on the surface area of the nanosheets. We found that the treatment increased the surface area of the nanosheets slightly from 19.96 m^2/g in untreated CuO to 24.56, 22.83, 22.29, and 24.72 m^2/g for toluene, *p*-xylene-, hexane-, and MCH-treated samples, respectively. The results are detailed in Table S2. Due to sample constraints, we could not determine the surface area of samples treated with CB. On the basis of this data, we find no correlation between the type of treatment and the change in surface area. In particular, aromatic rings increase the surface area as much as cyclic or linear alkanes. The TEM images suggest that the increase in surface area observed in treated samples is due to the presence of large defects, likely a product of the functionalization procedure.

Surface area can change the contact angle observed for a material.[50] However, increases in surface area would make a hydrophilic surface more hydrophilic and a hydrophobic surface more hydrophobic. In this work, we see a shift from hydrophilicity in the untreated sample, to the point where it absorbs water, toward more hydrophobicity in all treated samples. Additionally, there is no trend in surface area with hydrophobicity in the treated samples. Therefore, the changes in surface area cannot be solely responsible for the changes in contact angle.

Another factor that plays a critical role in hydrophobicity is the composition of the material. Cuprous oxide is well-known for being hydrophobic,[66] however its poor stability limits its utilization in many applications. XRD was performed to determine if the treatment converted any of the CuO materials into Cu_2O. Since CuO and Cu_2O have very distinct diffraction patterns, they are easily distinguishable in XRD. All samples, treated and untreated, were found to have diffraction patterns matching that of CuO (Powder Diffraction File (PDF) No.: 01−080−1268, Joint Committee on Powder Diffraction Standards (JCPDS), [year], Figure S2). No Cu_2O peaks were detected, indicating that the crystal structure and composition were that of CuO. The peak broadening found in all samples is consistent and expected due to nanosized crystallite domains. Calculations of the size of the crystallite domains, based on Scherrer's equation, are consistent with the nanoscale observed in previous work.[51] On the basis of this data, we conclude that the increases in hydrophobicity are not due to changes in nanostructure or bulk composition.

Surface Chemistry. Having found no significant changes to the nanostructure or crystal structure, we turned our attention toward the surface composition. To determine how the functionalizing species bind to the surface, we first performed FTIR measurements (Figure 3). Though typically considered only a surface technique, the penetration depth of FTIR-ATR

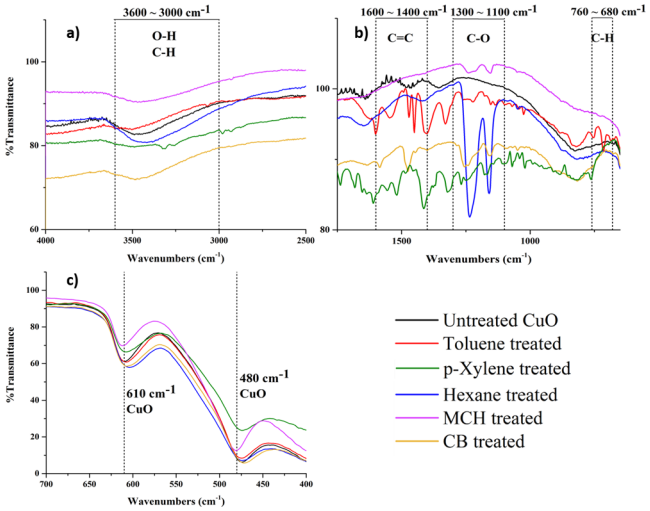

Figure 3. (a) FTIR spectra of all samples in 2500−4000 cm^{-1},; (b) fingerprint region spectra from 650 to 1750 cm^{-1}. C−O bonds were observed in all functionalized samples indicating the oxidation of the organic adsorbates. (c) Characteristic IR adsorption peaks for CuO at 610 and 480 cm^{-1}.

DOI: 10.1021/jacs.7b11654
J. Am. Chem. Soc. 2018, 140, 1824−1833

can range from 0.5 to 2.0 μm. Since the thickness of the CuO nanosheets is on the order of 10−20 nm, this technique is likely probing tens to hundreds of nanosheets. Nevertheless, noncrystalline surface groups may still be detected using this technique.

Untreated CuO nanosheets displayed strong peaks at 480 and 610 cm^{-1}, consistent with literature sources (Figure 3).[67] Those peaks are associated with Cu−O stretching. A broad peak is also visible in the region around 3500 cm^{-1}, typical of O−H stretching. Toluene-treated CuO nanosheets showed not only the same two characteristic peaks as those of the untreated sample but also additional ones. In the range of 1400−1600 cm^{-1}, we see peaks at 1600, 1560, 1480, and 1450 cm^{-1}. This energy range is typically associated with C═C aromatic skeleton vibrations. Additionally, C−H wagging absorptions of benzene rings at 760 and 710 cm^{-1} are detected. Similar peaks can be found in the *p*-xylene functionalized sample at 1600, 1580, 1520, and 1450 cm^{-1} as well as C−H wagging peak at 760 cm^{-1}. Furthermore, in the toluene-treated sample we also see a peak at 3100 cm^{-1} corresponding to unsaturated C−H stretching. In the *p*-xylene sample we see multiple C−H stretching peaks above and below 3000 cm^{-1}, indicative of both saturated and unsaturated C−H bond stretching. The observed vibrational features strongly imply that the aromatic rings of the adsorbates remain intact after the functionalization. Interestingly, these spectra are not simply the superposition of CuO nanosheets and the solvent used for functionalization. In the toluene-treated samples at 1260 and 1158 cm^{-1} as well as in the *p*-xylene-treated samples at 1266 and 1174 cm^{-1}, we see peaks frequently attributed to C−O bond stretching. Since there are no C−O bonds present in the molecular precursors, those vibrational bands suggest that the precursors are oxidized and covalently bonded as alkoxides to the CuO nanosheets.

The FTIR spectra of CuO nanosheets treated with hexane and MCH are very similar. Both exhibit the characteristic CuO peaks as well as peaks in the 1100−1300 cm^{-1} range corresponding to C−O bonds, as for the C−O stretching of aromatic-treated samples. However, no peaks associated with aromatics are found, nor expected, since the precursors do not include aromatic functional groups. Differences also exist in the hydroxyl stretching regions at 3500 cm^{-1}. While the peak intensity was drastically attenuated for toluene- and *p*-xylene-treated samples compared to the untreated CuO nanosheets, the hydroxyl region changed very little for MCH- and hexane-treated samples. In fact, as suggested by modeling analysis discussed in greater details in the following section, the C−O stretching peaks in these cases are more likely to be ascribed to the hydroxyl groups that formed in the carbon framework after being oxidized by the CuO nanosheets.

Turning our attention to the CB-treated CuO nanosheets, we find significantly fewer peaks in the FTIR spectrum compared to toluene- or *p*-xylene-treated nanosheets. The aromatic C═C stretching peaks were much more attenuated and many benzene structure related peaks have disappeared, including the benzene skeleton stretching at 1447 cm^{-1}, unsaturated C−H stretching at 3067 cm^{-1}, and C−H wagging peaks of aromatics at 704 and 686 cm^{-1}. Additionally, no C−Cl stretching signal (742 cm^{-1}) was detected after functionalization, indicating the abstraction of chlorine during the reaction, consistent with the earlier observation of CB decomposition over mesostructured CuO catalysts.[41] Though in that study CB degradation occurs at a higher temperature (250 °C), we find that CuO nanosheets are more reactive than their bulk counterparts.[51] Therefore, we conclude that CB has decomposed over the CuO nanosheets during reflux. This might indicate that the low contact angle observed for the CB-treated sample, compared to the toluene- or *p*-xylene-treated samples, is due to structural loss of the aromatic ring. Similar to the other samples, we find C−O stretching around 1250 cm^{-1}, further indicative of oxidation of the functional groups.

XPS was performed to further probe and compare the surfaces of treated and untreated CuO nanosheets (Figure 4).

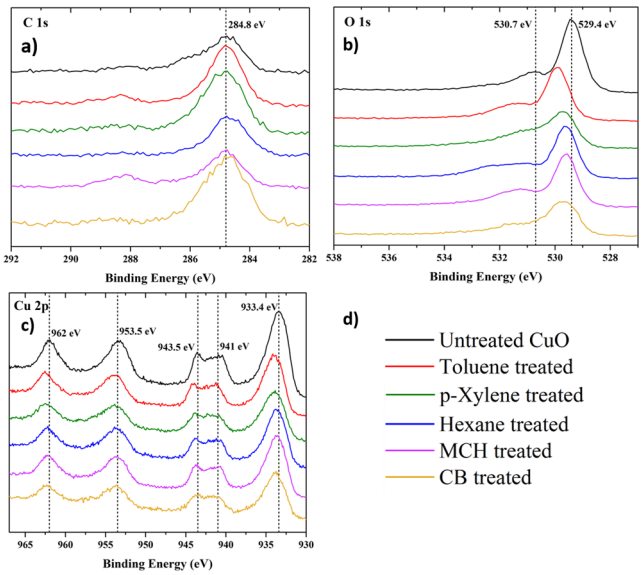

Figure 4. XPS regional spectra for all samples: (a) C 1s, (b) O 1s, and (c) Cu 2p; (d) color codes. All spectra were calibrated to C 1s 284.8 eV. Compared to untreated CuO, all functionalized samples exhibited a higher C 1s peak and lower O 1s and Cu 2p peaks, indicating an increase in the carbon surface coverage.

Experimental details are given in the Supporting Information. All the spectra were similar at Cu 2p, displaying the characteristic peaks at 933.4, 941 eV and 943.5, 953.5, and 962 eV corresponding to Cu $2p_{3/2}$ and Cu $2p_{3/2}$ satellite peaks and Cu $2p_{1/2}$ and Cu $2p_{1/2}$ satellite peaks, respectively. No peaks were found corresponding to Cu^{1+} or Cu^{0} in any of the samples. This suggests that the treatments do not reduce the nanosheets to cuprous oxide or copper metal, which is consistent with the XRD and FTIR data. One difference is that qualitatively all of these peaks are lower in intensity in the functionalized samples compared to the untreated sample. The implications of this will be discussed quantitatively after examining oxygen and carbon.

At O 1s, we find significant differences in the spectra of treated and untreated CuO nanosheets samples. For the untreated CuO nanosheets, we find two characteristic binding energy peaks at 529.4 and 530.7 eV, which correspond to lattice oxygen and hydroxyl groups, respectively. In all cases, functionalization of CuO nanosheets with small organic molecules shifted the O 1s peak toward higher binding energy. For toluene-treated sample, the binding energy is shifted to 530 eV, and for the other treatments, the binding energy is shifted to 529.7 eV. In the case of *p*-xylene, a small shoulder is visible at 531 eV. The peak typically associated with surface hydroxyl groups is also shifted in all treated samples. It appears at 531.5 eV for toluene- and MCH-treated nanosheets, as a shoulder at 531 eV for the *p*-xylene-treated nanosheets, and as a plateau

DOI: 10.1021/jacs.7b11654
J. Am. Chem. Soc. 2018, 140, 1824−1833

from 531 to 532 eV for CB-treated nanosheets and from 530.5 to 533.5 eV for hexane-treated nanosheets. In addition, the peak areas of hydroxyl groups are lower in toluene- and *p*-xylene-treated samples compared to other functionalized and untreated samples, consistent with the FTIR data. We hypothesize that the differences in the spectra especially in this region results from the wide array of ways oxygen is bonded. Nonspecific oxidation of the hydrocarbon functional groups would result in the presence of many different oxygen species. This view is also supported by the FTIR data where peaks for many different types of bonds were present. Interestingly, as we will discuss quantitatively, the intensities of these peaks are not correlated to the contact angle of the material. This would suggest that hydrophobicity is not simply a matter of surface coverage, but relates to the complex surface chemistry of each functional group on the surface of the material.

More information can be gained from the C 1s region of the spectra. Here the intensities of the peak at 284.8 eV are different; CB-treated CuO nanosheets have the largest peak intensity followed by toluene- and *p*-xylene-treated samples, then the hexane-treated sample, the MCH-treated sample, and finally the untreated sample with the lowest peak intensity. Interestingly, we see differences in the peak at 288.5 eV, which is typically associated with O−C═O. Here, the MCH-treated sample has the largest peak, followed by the toluene, then the *p*-xylene and untreated samples and the CB and hexane samples, which appear to have no signal in this region.

Shifts in binding energy relate to changes in the intramolecular atomic bonds. A shift to higher binding energies suggests that these bonds are becoming stronger, and shifts to lower binding energies suggests these bonds are weakening. In the case of the treated samples, it would appear that some of the oxygen atoms in the CuO structure are binding more strongly. Interestingly, we do not see these shifts at Cu 2p or C 1s. As mentioned above, the binding energy of carbon is calibrated and fixed at 284.8 eV. Therefore, small changes in chemical bonds within the material may not be apparent at C 1s. Cu 2p, however, is not as fixed. Indeed, others have shown that even small changes in the oxidation state of copper can significantly alter the peaks intensity and position at Cu 2p.[68] This leads us to conclude that functional groups are likely binding through lattice oxygen atoms rather than copper atoms.

A quantitative analysis of these spectra lends to more insights into the surface binding of these species, as shown in Table 1.

Table 1. Atomic Concentration Calculated from XPS

atomic concentration	C%	O%	Cu%	Cu/O	C/O
untreated CuO	15.43	41.70	42.88	1.03:1	0.37:1
toluene-treated	24.87	39.82	35.31	0.89:1	0.62:1
p-xylene-treated	30.65	37.85	31.50	0.83:1	0.81:1
hexane-treated	19.11	44.78	36.11	0.81:1	0.43:1
MCH-treated	20.66	40.95	38.40	0.94:1	0.5:1
CB-treated	36.57	33.44	29.99	0.9:1	1.09:1

In the untreated CuO sample we calculate that there is 15.4% carbon relative to oxygen and copper by atom. For functionalized samples, we find that this number grows to 24.9% in the toluene-treated sample, 30.7% in the *p*-xylene-treated sample, 19.1% in the hexane-treated sample, 20.7% in the MCH-treated sample, and 36.6% in the CB-treated sample. In general, there is some relation between hydrophobicity and carbon content; toluene and *p*-xylene contain 5−10% more carbon than the hexane and MCH samples. The exception to the rule is CB-treated copper oxide, which has the highest carbon percent and a hydrophobicity only on par with hexane- and MCH-treated copper oxide. Also of note is that no chlorine was detected in any of the samples, including the CB-treated CuO nanosheets. This is consistent with the FTIR spectra for CB-treated CuO nanosheets that showed no C−Cl signals. On the basis of this evidence, we must conclude that the CB is being decomposed by the CuO nanosheets during the functionalization treatment. The difference in hydrophobicity, therefore, cannot simply be a function of carbon surface coverage, but also must be due to the arrangement of carbon on the surface. This further supports the conclusions being drawn on the basis of the FTIR data that the presence of aromatic rings greatly enhances hydrophobicity.

Since the percent of carbon in all treated samples changed relative to that of the untreated sample, the oxygen and copper percentages also by necessity have to change. In all cases, the percentage of these atoms decreased relative to the untreated sample, however not by the same amount. In the untreated sample, the copper to oxygen ratio is 1.03:1; in the toluene-treated sample, the ratio is 0.89:1, In the *p*-xylene-treated sample, the ratio is 0.83:1; in the hexane-treated sample, the ratio is 0.81:1. In the MCH-treated sample, the ratio is 0.94:1; in the CB-treated sample, the ratio is 0.9:1. This ratio does not follow a trend in the hydrophobicity, nor does it correlate to overall carbon coverage. However, what is consistent is that all-treated samples have less copper than oxygen.

On the surface, this result is quite surprising. Previously, we just concluded that lattice oxygen is binding these functional groups and that these hydrocarbons can be oxidized by them. If one would predict atoms to be lost, then one might expect it would be oxygen atoms, perhaps assuming that a portion of the oxidized hydrocarbons dissociate from the surface, leaving a copper-rich, cuprous environment. Yet we find the opposite is true; that is, we find more oxygen atoms than copper atoms.

In the past, we have reported other treatments that have increased the ratio of oxygen relative to copper.[51] In this work, however, we believe the mechanism to be completely different. In aqueous environments, copper is known to leach into the solution forming copper ions.[69] Here, although the treatments occur in organic solvents, we suspect a similar process may be at play. X-ray fluorescence was used to test this theory, as shown in Figure S3. After treatment, the solution was filtered, and the filtrate was collected and drop-cast onto filter paper in order to measure the presence of copper in solution. We detected a signal at 2θ equal to 45°, corresponding to a Cu Kα edge at 8.040 keV. This suggests that the Cu atoms are leaching into the solvent during the functionalization treatment, possibly related to a redox reaction occurring at the surface, that is, after the solvent is oxidized, the remaining copper atom becomes less stable since it is coordinated by fewer oxygen atoms causing it to leach into solution. We conducted EPR measurements of the toluene solution after treatment, but could not detect any Cu^{2+} (data not shown) suggesting that if copper is leaching then it is likely in the 1+ or 0 oxidation state. From XRD we know that the crystal structure of the material is unchanged, so this leaching must only be occurring on the surface resulting in defects observed during TEM. Finally, we also conclude that this is the cause behind the substoichiometric ratio of Cu to O in the treated CuO nanosheet samples observed during XPS.

Further information can be gained by taking the ratio between carbon to oxygen atoms. Here, we find that the ratio of

DOI: 10.1021/jacs.7b11654
J. Am. Chem. Soc. 2018, 140, 1824−1833

carbon to oxygen atoms in the CB-treated sample is the greatest with a value of 1.09:1, followed by the *p*-xylene-treated sample with a value of 0.81:1, the toluene-treated sample with a value of 0.62:1, the MCH-treated sample with a value of 0.50:1, the hexane-treated sample with a value of 0.43:1, and finally by the untreated sample with a value of 0.37:1. Compared to the Cu/O ratio, the C/O ratio is a much better indicator of the material's hydrophobicity. The *p*-xylene-treated sample is more hydrophobic than the toluene sample and has a greater C/O ratio and both are greater than those of the hexane- and MCH-treated samples, which is consistent with the trend in contact angle. Lower C/O ratio, such as in the case of hexane- and MCH-treated samples, may be due to increased oxidation of the functional groups leading to increased potential for hydrogen bonding in solution and consequently a lower hydrophobicity and contact angle. The outlier here seems to be the CB sample, with the highest C/O ratio and the lowest contact angle. This indicates that while the C/O ratio can be a useful tool in predicting the hydrophobicity it is not sufficient. Other factors, such as the retention of the aromatic ring, is necessary to consider when tuning the hydrophobicity of the surface.

Binding Mechanism. Our FTIR spectra suggested the presence of C−O bonds in all treated samples, consistent with previous studies which show that CuO catalyzes the oxidation of toluene and cyclohexane to $PhCH_2OH$[70] and cyclohexanol,[42] respectively. In addition, Kaliszewski and Heuer[71] studied the interaction between ethanol and hydrous zirconia powders by FTIR spectroscopy and provided evidence of ethoxide formation, attributed to dehydration of CH_3CH_2OH and surface Zr−OH groups. On the basis of our FTIR spectra and previous studies, we proposed a functionalization mechanism shown in Figure 5a. The reaction involves partial

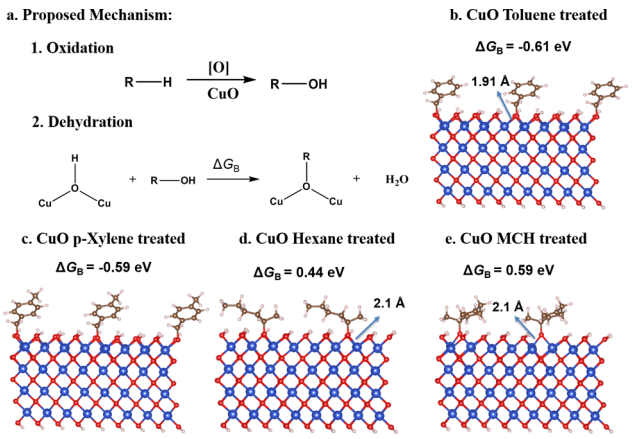

Figure 5. (a) Proposed mechanism of surface functionalization of CuO treated by organic solvents. Structures and calculated binding free energies of (b) toluene-, (c) *p*-xylene-, (d) hexane-, and (e) MCH-treated CuO surfaces.

oxidation of organic molecules (R−H) to alcohols (R−OH). The alcohols then dehydrate with the surface hydroxyl groups of CuO to form surface-bound Cu−O−R, responsible for the hydrophobicity of functionalized CuO nanosheets. Our DFT calculations support the proposed mechanism and rationalize the observed water contact angles and FTIR spectra of various treated CuO samples.

We considered five organic molecules, namely, toluene, *p*-xylene, hexane, MCH, and CB. CuO nanosheets were modeled with the hydroxyl-terminated CuO (002) surface to be consistent with previous XRD and band gap measurements,[51] as well as FTIR spectra in the current study. The oxidation of all five molecules by oxygen to form alcohols is found to be thermodynamically favorable, with negative reaction free energies (See Figure S4). Thus, the reaction between R−OH and the Cu−OH surface to form Cu−O−R and H_2O is the most relevant step, and the corresponding binding free energy (ΔG_B) determines whether the hydrophilic Cu−OH surface can be modified by the hydrophobic R groups to form hydrophobic Cu−O−R surface. For toluene and *p*-xylene, the proposed alcohol intermediates are $PhCH_2OH$ and CH_3−Ph−CH_2OH, respectively. Our calculated binding ΔG_B of $PhCH_2OH$ and CH_3−Ph−CH_2OH on the CuO (002) surface are −0.61 and −0.59 eV, respectively. Therefore, $PhCH_2OH$ and CH_3−Ph−CH_2OH spontaneously bind to CuO surfaces and make it hydrophobic. On the basis of bond dissociation energies of primary, secondary, and tertiary C−H bonds,[72] the most likely partially oxidized alcohol intermediates for MCH and hexane would be 1-methyl-cyclohex-1-ol and 2-hexanol. Direct binding of 1-methyl-cyclohex-1-ol and 2-hexanol to CuO surfaces to form hydrophobic Cu−O−R groups is unlikely due to the large steric repulsions between alkyl groups near the C−O bond and CuO surfaces, as indicated by the large positive ΔG_B of 1-methyl-cyclohex-1-ol and 2-hexanol, 0.44 and 0.59 eV, respectively. In addition, a secondary aromatic alcohol α-methylbenzyl alcohol model was computed to test this hypothesis, and results showed that the dehydration of α-methylbenzyl alcohol on CuO surface has a positive free energy change of 0.10 eV (Figure S5) due to the large steric repulsion, indicating that the steric factor plays an important role in determining the hydrophobicity. Instead of dehydration, the partially oxidized intermediates (1-methyl-cyclohex-1-ol and 2-hexanol) and CuO surfaces could form hydrogen-bonding complexes with a negative free energy change of −0.17 and −0.28 eV (Figure S6), which may slightly modify the water contact angles compared to the untreated CuO nanosheets.

For CB, there is no position with methyl, secondary, and/or tertiary C−H bonds to be oxidized; thus, the functionalization of CuO surfaces with CB is likely to undergo a different pathway. FTIR analysis and previous studies have suggested that CB is decomposed into nonaromatic compounds over CuO nanosheets, thus resulting in only a slight increase in the water contact angle, similar to the cases of MCH and hexane functionalization.

Our computational results suggest that the hydrophobicity of CuO nanosheets treated with toluene and *p*-xylene comes from the reaction of surface hydroxyl groups with R−OH intermediates (R = $PhCH_2$ for toluene and R = CH_3−Ph−CH_2 for *p*-xylene), which changes hydrophilic Cu−OH surface groups into hydrophobic Cu−O−R groups. During the functionalization process, CuO nanosheets first catalyze the oxidation of toluene and *p*-xylene to $PhCH_2OH$ and CH_3−Ph−CH_2OH, respectively. The *in situ*-generated $PhCH_2OH$ and CH_3−Ph−CH_2OH then react with the surface Cu−OH groups and bind as alkoxides Cu−O−R. Our results suggest that we can directly use aromatic structures with oxidizable groups such as toluene and *p*-xylene to modify the CuO surface groups to make it hydrophobic. The resulting functionalization should also be applicable to other metal oxides.

Since the proposed mechanism suggests that the dehydration between −OH and Cu−OH leads to the hydrophobicity, one might think that similar chemistry would occur with other

DOI: 10.1021/jacs.7b11654
J. Am. Chem. Soc. 2018, 140, 1824−1833

alcohol precusors. CuO nanosheets were functionalized with benzyl alcohol to test this hypothesis; however, the contact angle of this material was found to be only 33°. Note that the reaction was kept at the boiling temperature of toluene instead of that of benzyl alcohol because under reflux conditions benzyl alcohol showed the capability of fully reducing the CuO nanosheets into Cu metals. We suspect that benzyl alcohol is oxidized further to benzyl aldehyde leading to unfavorable reactivity with the surface.

Our DFT calculations show that benzyl aldehyde does not favorably bind to the surface. To further understand the underlying chemistry, we performed proton-nuclear magnetic resonance spectroscopy. The liquid phases before and after functionalization in toluene and benzyl alcohol systems were collected and analyzed using ^{1}H NMR. After refluxing for 24 h, both samples exhibited significant changes in compositions as revealed by NMR spectra, Figure S7. Toluene was found to be partially oxidized into benzyl alcohol and benzaldehyde at trace quantities, given by the presence of additional peaks associated with benzyl alcohol and benzaldehyde in NMR after functionalization. These results are consistent with our DFT-proposed mechanism and earlier work suggesting that CuO was capable of oxidizing gaseous toluene into benzyl alcohol, benzaldehyde, benzoic acid, and other molecules.[44]

The conversion of benzyl alcohol to benzaldehyde in the liquid phase was found to be 6%, which is significant compared to the toluene functionalization case where the conversion to benzyl alcohol is less than 1%. This suggests that when reacting with CuO nanosheets benzyl alcohol is more reactive than toluene and therefore can be more easily oxidized into benzyl aldehyde. On the basis of that observation, along with our calculations showing that the Gibbs free energy change of benzyl aldehyde binding to CuO nanosheets surface is not as favorable as that of benzyl alcohol, we conclude benzyl alcohol is oxidized into benzyl aldehyde in the functionalization process and therefore does not favorably bind to the surface, resulting in the small contact angle change (Figure S8).

^{1}H NMR studies suggest that redox chemistry is occurring between the solvent and the CuO nanosheets during functionalization and that oxidation of the solvent is essential for functionalization. The result of these reactions is key for determining the binding strength of the functional group, the chemical composition of the functional group, and the hydrophobicity of the resulting material.

Stability and Surface Coverage. Thermogravimetric analysis (TGA) was performed in air to test thermal stabilities of treated and untreated CuO nanosheets, Figure S9. Absolute weight loss and derivative weight loss percent is graphed as a function of temperature. Compared to the untreated sample, all functionalized samples were found to have significant weight loss. This weight loss occurred way above the boiling points of the functional groups' corresponding solvent, evidencing the claim that functional groups in the treated samples are strongly bonded to the surface of the CuO nanosheets. That being said, there are significant differences between the TGA plots of the various treated samples (Table 2).

The *p*-xylene- and toluene-treated samples were found to be the most stable, showing no significant weight loss below 350 °C. Sharp peaks in the derivative weight loss percent can be seen at 356 and 350 °C for *p*-xylene- and toluene-treated samples, respectively. Importantly, these are the only peaks found in these samples, indicating that a single species is decomposing or desorbing from the surface. The hexane-, MCH-, and CB-treated samples were found to be less stable, showing derivative peaks at 300, 306, and 325 °C, respectively. Unlike the toluene- and *p*-xylene-treated samples, these samples display broad peaks in their derivative plots. Additionally, these materials also show additional broad peaks over the range of 400−500 °C. This suggests that there are possibly multiple species on the surface and/or the decomposition of these species is a multistep process. Qualitative inspection of the plots suggests that there is correlation between the shapes of these peaks and the hydrophobicity of the material. That is, the toluene- and *p*-xylene-treated samples have sharp single peaks with temperatures above that of the broad peaks of the hexane-, MCH-, and CB-treated samples.

Table 2. Surface Coverage Calculated from BET and TGA

samples	derivative weight peak location (°C)	mass ratio (%)	surface coverage (mg/m^2)
untreated	400−500	0.34	0.17
toluene-treated	350	1.08	0.44
p-xylene-treated	356	1.38	0.60
hexane-treated	300	1.26	0.57
MCH-treated	306	1.84	0.74
CB-treated	325	1.65	0.70[a]

[a]The surface coverage of CB treated sample was calculated using the averaged surface areas of other samples due to the sample constraint.

The untreated sample was found to have only a small, broad peak in the derivative plot spanning from 400 to 500 °C. It is difficult to conclude what this peak may be caused by. Though its position is similar to some of the other functionalized samples, its low intensity indicates that it is related to a separate process, such as oxygen exchange between the gas and solid phase.[51] It is unlikely that any cuprous oxide is forming since the in air cupric oxide is more thermodynamically stable. A small baseline increase is found for all samples; this is an artifact of the instrument and is more pronounced when there is low absolute mass loss, as in the case of the untreated sample, or low sample loading, which was the case for the toluene-treated sample due to sample constraints.

A quantitative analysis can be made by assuming that the mass loss in a sample is only a result of desorption of the functional groups. By doing so we can calculate the percent by mass of the functional groups for each sample (Table 2). The peaks in the derivative plots were integrated and summed in cases where more than one peak was present, and we found that the functional groups mass percent ranged between 1 and 2% for all the treated sample. As a control, this calculation was also performed for the untreated sample; the mass loss calculated by this method for the untreated sample was found to be 0.34%, a factor of 3 less than any functionalized sample. The MCH-functionalized CuO nanosheets were found to have the greatest functional group mass percent with a value of 1.84%, the CB-treated sample had the second highest with a value of 1.65%, followed by the *p*-xylene-treated sample with 1.38%, the hexane-treated sample with 1.26%, and finally the toluene-treated sample with a functional group mass percent of 1.08%.

Further information can be gained by combining these TGA weight loss results with BET surface area measurements discussed earlier. We can calculate the surface coverage of the functional groups on the treated samples using

DOI: 10.1021/jacs.7b11654
J. Am. Chem. Soc. 2018, 140, 1824−1833

$$\frac{M_f}{\sigma} = \tau \quad (1)$$

where M_f is the mass fraction of the functional group compared to the overall sample ($g_{\text{functional group}}/g_{\text{total}}$), σ is the specific surface area of the sample (m^2/g_{total}), and τ is the surface coverage ($g_{\text{functional group}}/m^2$). More information on calculations can be found in the Supporting Information, page S6.

The values for surface coverage are reported in Table 2. Surprisingly, we find that the MCH-treated sample had the highest surface coverage with a value of 0.74 mg/m^2, followed by the CB-, *p*-xylene-, hexane-, and toluene-treated samples, with values of 0.70, 0.60, 0.57, and 0.44 mg/m^2, respectively. For comparison, the untreated sample was calculated to have a surface coverage of 0.17 mg/m^2, more than a factor of 2 less than any of the functionalized samples.

Most surprisingly, we find that contact angle is not correlated with a sample's functional group mass percent or its surface coverage. The toluene-treated sample, which showed one of the highest contact angle, in fact showed the lowest surface coverage and functional group mass percent, and the hexane sample with a high functional group mass percent and the highest surface coverage showed only a small increase in contact angle compared to the untreated sample. This suggests that the surface chemistry plays a major factor in determining the hydrophobicity of the material. That is, surface aromatic groups lead to a higher hydrophobicity.

We performed H_2-TPR to determine the stability of these materials (more information can be found in the Supporting Information, page S16). First, 20 mg of treated and untreated CuO nanosheets were heated in H_2 gas from 100 to 400 °C at 10 °C per min in a straight tube reactor. We used online mass spectrometry to monitor the outlet gas composition and observe H_2 consumption. Upon heating, CuO reacts with H_2 gas to form H_2O and Cu metal, as described by the following chemical equation:

$$CuO_{(s)} + H_{2(g)} \rightarrow Cu_{(s)} + H_2O_{(g)} \quad (2)$$

Percent H_2 consumption for treated and untreated CuO nanosheets are plotted as a function of temperature in Figure 6. A peak for H_2 consumption occurs because increases in temperature lead to increases in reaction rate, but depletion of oxygen within the CuO causes a sharp extinction of the reaction. A single peak is observed, as opposed to two peaks, because reduction of CuO with H_2 leads directly to copper metal without passing through Cu_2O.[73] In the past, we have used peak H_2 consumption temperature as a measure of the reactivity and stability of CuO nanosheets.[51] That is, a lower peak H_2 consumption temperature is indicative of a more reactive material, but a higher peak H_2 consumption temperature of a more stable one.

In Figure 6, we find peaks for H_2 consumption located at different temperatures depending on the treatment. The untreated sample has the lowest peak H_2 consumption temperature at 235 °C. This is similar to previous work,[51] though slightly lower, likely due to differences in sample loading (20 mg in this work versus 50 mg in previous work). A lower sample loading results in a lower signal-to-noise ratio, though was necessary for this work due to sample constraints.

Peak percent H_2 consumption peaks for the treated samples are located at 286, 295, 322, 327, and 334 °C for the CB-, hexane-, MCH-, toluene-, and *p*-xylene-treated samples, respectively. Therefore, the *p*-xylene-treated CuO nanosheets

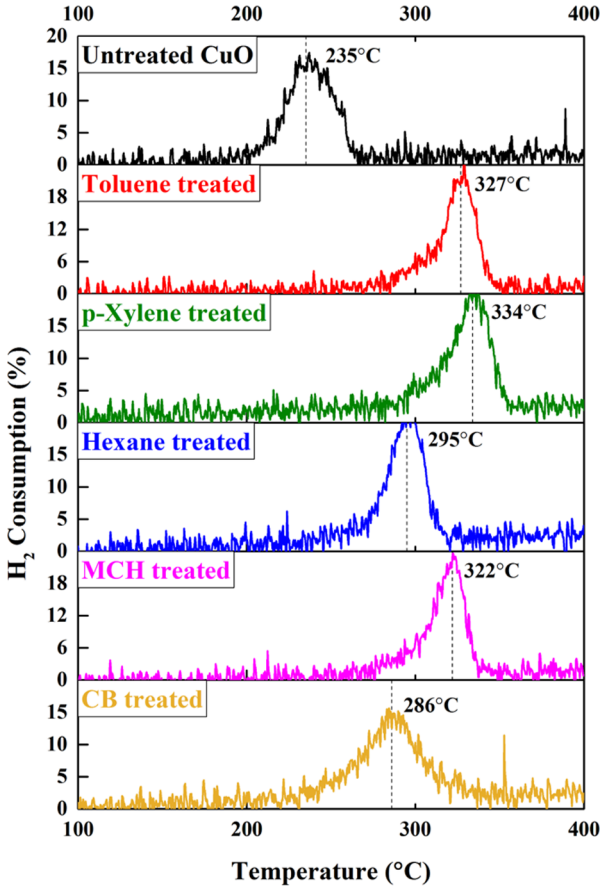

Figure 6. Temperature-programmed reduction profiles from top to bottom: untreated CuO nanosheets; toluene-treated, *p*-xylene-treated, hexane-treated, MCH-treated, and CB-treated CuO nanosheets. The peak location correlates with the hydrophobicity.

are more stable than the toluene-treated CuO nanosheets, which are more stable than the MCH-treated CuO nanosheets, followed by the hexane-treated CuO nanosheets, the CB-treated CuO nanosheets, and finally by the untreated CuO nanosheets. Interestingly, this trend seems to correlate very well with the trend in contact angles, that is, the more hydrophobic samples are more stable.

The location of H_2 TPR consumption peaks correlates with properties such as band gap that can be tuned with changes to the surface of the CuO nanosheets. Therefore, the trend we find with hydrophobicity is further evidence of property-property relationships likely linked to sensitive surface states in the CuO nanosheet system.

■ CONCLUSION

We have introduced hydrophobic CuO nanosheets by functionalization with hydrophobic organic molecules, such as toluene, *p*-xylene, hexane, MCH, and CB. We found that these groups can increase the hydrophobicity of the nanosheets up to a contact angle of 146°. We showed that the functionalization treatments alter the properties of the surface without changing the nanostructure or crystal structure of CuO. Our experimental and computational tools determined that methylated aromatics (e.g., toluene and *p*-xylene) are first oxidized by CuO and then bind to the surface as alkoxides. Other chemicals, such as hexane and MCH are oxidized as well, though their binding is weaker. We determined that the surface

DOI: 10.1021/jacs.7b11654
J. Am. Chem. Soc. 2018, 140, 1824−1833

coverage of these species is not correlated with the hydrophobicity of the material; rather, aromatic groups on the CuO surface play a more significant role in introducing hydrophobicity. Through TGA and H_2-TPR we find these surface groups are stable up to 300 °C. Hydrophobicity and H_2-TPR reactivity are correlated properties in this system. We determined that functional groups with methylated aromatic rings are ideal candidates for functionalizing CuO nanosheets. This strategy of small molecule functionalization has the potential to be applied to a wide range of metal oxides, for increasing their hydrophobicity and stability in various applications.

■ ASSOCIATED CONTENT

Supporting Information

The Supporting Information is available free of charge on the ACS Publications website at DOI: 10.1021/jacs.7b11654.

Characterization technique details, contact angles, SEM images showing no significant structural loss, BET physisorption calculations on surface area and surface coverage, X-ray diffraction showing no composition changes after functionalization, XPS operation details, XRF spectrum showing the existence of copper ions in the liquid phase, calculated Gibbs free energies for oxidation reactions, calculation on α-methylbenzyl alcohol, calculated binding free energies of hydrogen bonding complexes, ^{1}NMR calculation details, calculated benzyl aldehyde binding free energy, thermogravimetric analysis, temperature-programmed reduction (PDF)

■ AUTHOR INFORMATION

Corresponding Authors

*E-mail: victor.batista@yale.edu.

*E-mail: lisa.pfefferle@yale.edu

ORCID

Yulian He: 0000-0002-8994-1979

Victor S. Batista: 0000-0002-3262-1237

Author Contributions

Y.H. and Z.S.F. contributed equally to this work.

Funding

ARO grant #64935, Agreement W911NF1410564 AFOSR grant #FA9550-13-1-0020.

Notes

The authors declare no competing financial interest.

■ ACKNOWLEDGMENTS

Z.S.F., Y.H., and L.D.P. graciously thank the Army Research Laboratory for generous support of funding for this research under ARO grant #64935, Agreement W911NF1410564, and thank the YINQE and CRISP facilities for providing access to and assistance with TEM, SEM, and XRD instruments. K.R.Y and V.S.B acknowledge an allocation of high-performance computer time from the National Energy Research Scientific Computing Center (NERSC) and support by the Air Force Office of Scientific Research (AFOSR) grant #FA9550-13-1-0020. The project made use of the Chemical and Biophysical Instrumentation Center at Yale University. The XPS work was performed under the instruction of Dr. Min Li using PHI VersaProbe II X-ray Photoelectron Spectrometer at Yale West Campus Materials Characterization Core. Additionally, we acknowledge Dr. Taylor and his research group for providing us access to their TA Instruments Q50.

■ REFERENCES

(1) Kataura, H.; Kumazawa, Y.; Maniwa, Y.; Umezu, I.; Suzuki, S.; Ohtsuka, Y.; Achiba, Y. *Synth. Met.* **1999**, *103*, 2555−2558.

(2) Stewart, A.; Zheng, S.; McCourt, M. R.; Bell, S. E. *ACS Nano* **2012**, *6*, 3718−3726.

(3) Kolhatkar, A. G.; Jamison, A. C.; Litvinov, D.; Willson, R. C.; Lee, T. R. *Int. J. Mol. Sci.* **2013**, *14*, 15977−16009.

(4) Tang, Q.; Zhou, Z.; Chen, Z. *Nanoscale* **2013**, *5*, 4541−4583.

(5) Zhao, S.; Fathololoumi, S.; Bevan, K.; Liu, D.; Kibria, M. G.; Li, Q.; Wang, G.; Guo, H.; Mi, Z. *Nano Lett.* **2012**, *12*, 2877−2882.

(6) Barbosa, S.; Agrawal, A.; Rodríguez-Lorenzo, L.; Pastoriza-Santos, I.; Alvarez-Puebla, R. A.; Kornowski, A.; Weller, H.; Liz-Marzán, L. M. *Langmuir* **2010**, *26*, 14943−14950.

(7) Guardia, P.; Labarta, A.; Batlle, X. *J. Phys. Chem. C* **2011**, *115*, 390−396.

(8) Njoki, P. N.; Lim, I.-I. S.; Mott, D.; Park, H.-Y.; Khan, B.; Mishra, S.; Sujakumar, R.; Luo, J.; Zhong, C.-J. *J. Phys. Chem. C* **2007**, *111*, 14664−14669.

(9) Pereira, C.; Pereira, A. M.; Fernandes, C.; Rocha, M.; Mendes, R.; Fernández-García, M. P.; Guedes, A.; Tavares, P. B.; Grenèche, J.-M.; Araújo, J. o. P.; et al. *Chem. Mater.* **2012**, *24*, 1496−1504.

(10) Kim, S.-K.; Day, R. W.; Cahoon, J. F.; Kempa, T. J.; Song, K.-D.; Park, H.-G.; Lieber, C. M. *Nano Lett.* **2012**, *12*, 4971−4976.

(11) Zeng, J.; Zhang, Q.; Chen, J.; Xia, Y. *Nano Lett.* **2010**, *10*, 30−35.

(12) Aradi, B.; Ramos, L.; Deák, P.; Köhler, T.; Bechstedt, F.; Zhang, R.; Frauenheim, T. *Phys. Rev. B: Condens. Matter Mater. Phys.* **2007**, *76*, 035305.

(13) Balasubramanian, K.; Burghard, M. *Small* **2005**, *1*, 180−192.

(14) Chen, R. J.; Bangsaruntip, S.; Drouvalakis, K. A.; Kam, N. W. S.; Shim, M.; Li, Y.; Kim, W.; Utz, P. J.; Dai, H. *Proc. Natl. Acad. Sci. U. S. A.* **2003**, *100*, 4984−4989.

(15) Chen, R. J.; Zhang, Y.; Wang, D.; Dai, H. *J. Am. Chem. Soc.* **2001**, *123*, 3838−3839.

(16) Dyke, C. A.; Tour, J. M. *J. Am. Chem. Soc.* **2003**, *125*, 1156−1157.

(17) Georgakilas, V.; Bourlinos, A.; Gournis, D.; Tsoufis, T.; Trapalis, C.; Mateo-Alonso, A.; Prato, M. *J. Am. Chem. Soc.* **2008**, *130*, 8733−8740.

(18) Gilbertson, L. M.; Goodwin, D. G., Jr; Taylor, A. D.; Pfefferle, L.; Zimmerman, J. B. *Environ. Sci. Technol.* **2014**, *48*, 5938−5945.

(19) Pastine, S. J.; Okawa, D.; Kessler, B.; Rolandi, M.; Llorente, M.; Zettl, A.; Fréchet, J. M. *J. Am. Chem. Soc.* **2008**, *130*, 4238−4239.

(20) Strano, M. S.; Dyke, C. A.; Usrey, M. L.; Barone, P. W.; Allen, M. J.; Shan, H.; Kittrell, C.; Hauge, R. H.; Tour, J. M.; Smalley, R. E. *Science* **2003**, *301*, 1519−1522.

(21) Sun, Y.-P.; Fu, K.; Lin, Y.; Huang, W. *Acc. Chem. Res.* **2002**, *35*, 1096−1104.

(22) Abellán, G.; Schirowski, M.; Edelthalhammer, K. F.; Fickert, M.; Werbach, K.; Peterlik, H.; Hauke, F.; Hirsch, A. *J. Am. Chem. Soc.* **2017**, *139*, 5175−5182.

(23) Chan, C. K.; Beechem, T. E.; Ohta, T.; Brumbach, M. T.; Wheeler, D. R.; Stevenson, K. J. *J. Phys. Chem. C* **2013**, *117*, 12038−12044.

(24) Daukiya, L.; Mattioli, C.; Aubel, D.; Hajjar-Garreau, S.; Vonau, F.; Denys, E.; Reiter, G. n.; Fransson, J.; Perrin, E.; Bocquet, M.-L.; et al. *ACS Nano* **2017**, *11*, 627−634.

(25) Park, J.; Yan, M. *Acc. Chem. Res.* **2013**, *46*, 181−189.

(26) Shunaev, V. V.; Glukhova, O. E. *J. Phys. Chem. C* **2016**, *120*, 4145−4149.

(27) Dettlaff-Weglikowska, U.; Skákalová, V.; Graupner, R.; Jhang, S. H.; Kim, B. H.; Lee, H. J.; Ley, L.; Park, Y. W.; Berber, S.; Tománek, D.; et al. *J. Am. Chem. Soc.* **2005**, *127*, 5125−5131.

(28) Liu, X.; Atwater, M.; Wang, J.; Huo, Q. *Colloids Surf., B* **2007**, *58*, 3−7.

(29) Zhang, P.; Sham, T. *Appl. Phys. Lett.* **2002**, *81*, 736−738.

DOI: 10.1021/jacs.7b11654
J. Am. Chem. Soc. 2018, 140, 1824−1833

(30) Wang, J. *ChemPhysChem* **2009**, *10*, 1748−1755.
(31) Lu, A. H.; Salabas, E. e. L.; Schüth, F. *Angew. Chem., Int. Ed.* **2007**, *46*, 1222−1244.
(32) Perreault, F.; Oukarroum, A.; Melegari, S. P.; Matias, W. G.; Popovic, R. *Chemosphere* **2012**, *87*, 1388−1394.
(33) Gao, X.; Bao, J.; Pan, G.; Zhu, H.; Huang, P.; Wu, F.; Song, D. *J. Phys. Chem. B* **2004**, *108*, 5547−5551.
(34) Dow, W.-P.; Wang, Y.-P.; Huang, T.-J. *J. Catal.* **1996**, *160*, 155−170.
(35) Faure, B.; Salazar-Alvarez, G.; Ahniyaz, A.; Villaluenga, I.; Berriozabal, G.; De Miguel, Y. R.; Bergström, L. *Sci. Technol. Adv. Mater.* **2013**, *14*, 023001.
(36) Wooh, S.; Encinas, N.; Vollmer, D.; Butt, H. J. *Adv. Mater.* **2017**, *29*, 1604637.
(37) Ujjain, S. K.; Roy, P. K.; Kumar, S.; Singha, S.; Khare, K. *Sci. Rep.* **2016**, *6*, 35524 DOI: 10.1038/srep35524.
(38) Xu, N.; Sarkar, D. K.; Grant Chen, X.; Zhang, H.; Tong, W. *RSC Adv.* **2016**, *6*, 35466−35478.
(39) Crick, C. R.; Parkin, I. P. *J. Mater. Chem.* **2011**, *21*, 14712−14716.
(40) Azimi Pirsaraei, S. R.; Asilian Mahabadi, H.; Jonidi Jafari, A. *Iran. J. Catal.* **2016**, *6*, 431−438.
(41) He, C.; Men, G.; Yu, Y.; Pan, H.; Xu, B. *Water, Air, Soil Pollut.* **2015**, *226*, 57.
(42) Medina-Valtierra, J.; Ramírez-Ortiz, J.; Arroyo-Rojas, V. M.; Ruiz, F. *Appl. Catal., A* **2003**, *238*, 1−9.
(43) Nauert, S. L.; Schax, F.; Limberg, C.; Notestein, J. M. *J. Catal.* **2016**, *341*, 180−190.
(44) Li, X.; Xu, J.; Wang, F.; Gao, J.; Zhou, L.; Yang, G. *Catal. Lett.* **2006**, *108*, 137−140.
(45) Enright, R.; Miljkovic, N.; Dou, N.; Nam, Y.; Wang, E. N. *J. Heat Transfer* **2013**, *135*, 091304.
(46) Wu, C.-J.; Chang, C.-C.; Sheng, Y.-J.; Tsao, H.-K. *Langmuir* **2017**, *33*, 1326−1331.
(47) Lee, S.-M.; Kim, K.-S.; Pippel, E.; Kim, S.; Kim, J.-H.; Lee, H.-J. *J. Phys. Chem. C* **2012**, *116*, 2781−2790.
(48) Roach, P.; Shirtcliffe, N. J.; Newton, M. I. *Soft Matter* **2008**, *4*, 224−240.
(49) Fihri, A.; Bovero, E.; Al-Shahrani, A.; Al-Ghamdi, A.; Alabedi, G. *Colloids Surf., A* **2017**, *520*, 378−390.
(50) Simpson, J. T.; Hunter, S. R.; Aytug, T. *Rep. Prog. Phys.* **2015**, *78*, 086501.
(51) Fishman, Z. S.; Rudshteyn, B.; He, Y.; Liu, B.; Chaudhuri, S.; Askerka, M.; Haller, G. L.; Batista, V. S.; Pfefferle, L. D. *J. Am. Chem. Soc.* **2016**, *138*, 10978−10985.
(52) Kresse, G.; Hafner, J. *Phys. Rev. B: Condens. Matter Mater. Phys.* **1993**, *47*, 558−561.
(53) Kresse, G.; Hafner, J. *Phys. Rev. B: Condens. Matter Mater. Phys.* **1994**, *49*, 14251−14269.
(54) Kresse, G.; Furthmüller, J. *Comput. Mater. Sci.* **1996**, *6*, 15−50.
(55) Kresse, G.; Furthmüller, J. *Phys. Rev. B: Condens. Matter Mater. Phys.* **1996**, *54*, 11169−11186.
(56) Blöchl, P. E. *Phys. Rev. B: Condens. Matter Mater. Phys.* **1994**, *50*, 17953−17979.
(57) Kresse, G.; Joubert, D. *Phys. Rev. B: Condens. Matter Mater. Phys.* **1999**, *59*, 1758−1775.
(58) Perdew, J. P.; Burke, K.; Ernzerhof, M. *Phys. Rev. Lett.* **1996**, *77*, 3865−3868.
(59) Dudarev, S. L.; Botton, G. A.; Savrasov, S. Y.; Humphreys, C. J.; Sutton, A. P. *Phys. Rev. B: Condens. Matter Mater. Phys.* **1998**, *57*, 1505−1509.
(60) Grimme, S.; Antony, J.; Ehrlich, S.; Krieg, H. *J. Chem. Phys.* **2010**, *132*, 154104.
(61) Grimme, S.; Ehrlich, S.; Goerigk, L. *J. Comput. Chem.* **2011**, *32*, 1456−1465.
(62) Hariharan, P. C.; Pople, J. A. *Theor. Chem. Acc.* **1973**, *28*, 213−222.
(63) Frisch, M. J.; Trucks, G. W.; Schlegel, H. B.; Scuseria, G. E.; Robb, M. A.; Cheeseman, J. R.; Scalmani, G.; Barone, V.; Mennucci, B.; Petersson, G. A.; Nakatsuji, H.; Caricato, M.; Li, X.; Hratchian, H. P.; Izmaylov, A. F.; Bloino, J.; Zheng, G.; Sonnenberg, J. L.; Hada, M.; Ehara, M.; Toyota, K.; Fukuda, R.; Hasegawa, J.; Ishida, M.; Nakajima, T.; Honda, Y.; Kitao, O.; Nakai, H.; Vreven, T.; Montgomery, J. A., Jr.; Peralta, J. E.; Ogliaro, F.; Bearpark, M.; Heyd, J. J.; Brothers, E.; Kudin, K. N.; Staroverov, V. N.; Kobayashi, R.; Normand, J.; Raghavachari, K.; Rendell, A.; Burant, J. C.; Iyengar, S. S.; Tomasi, J.; Cossi, M.; Rega, N.; Millam, J. M.; Klene, M.; Knox, J. E.; Cross, J. B.; Bakken, V.; Adamo, C.; Jaramillo, J.; Gomperts, R.; Stratmann, R. E.; Yazyev, O.; Austin, A. J.; Cammi, R.; Pomelli, C.; Ochterski, J. W.; Martin, R. L.; Morokuma, K.; Zakrzewski, V. G.; Voth, G. A.; Salvador, P.; Dannenberg, J. J.; Dapprich, S.; Daniels, A. D.; Farkas, O.; Foresman, J. B.; Ortiz, J. V.; Cioslowski, J.; Fox, D. J. *Gaussian 09*, revision E.01; Gaussian, Inc.: Wallingford, CT, 2009.
(64) Ribeiro, R. F.; Marenich, A. V.; Cramer, C. J.; Truhlar, D. G. *J. Phys. Chem. B* **2011**, *115*, 14556−14562.
(65) Momma, K.; Izumi, F. *J. Appl. Crystallogr.* **2011**, *44*, 1272−1276.
(66) Shinde, S. L.; Nanda, K. K. *RSC Adv.* **2012**, *2*, 3647−3650.
(67) Narang, S. N.; Kartha, V. B.; Patel, N. D. *Phys. C* **1992**, *204*, 8−14.
(68) Poulston, S.; Parlett, P.; Stone, P.; Bowker, M. *Surf. Interface Anal.* **1996**, *24*, 811−820.
(69) Gilbertson, L. M.; Albalghiti, E. M.; Fishman, Z. S.; Perreault, F.; Corredor, C.; Posner, J. D.; Elimelech, M.; Pfefferle, L. D.; Zimmerman, J. B. *Environ. Sci. Technol.* **2016**, *50*, 3975−3984.
(70) Li, X.; Xu, J.; Wang, F.; Gao, J.; Zhou, L.; Yang, G. *Catal. Lett.* **2006**, *108*, 137−140.
(71) Kaliszewski, M. S.; Heuer, A. H. *J. Am. Ceram. Soc.* **1990**, *73*, 1504−1509.
(72) Blanksby, S. J.; Ellison, G. B. *Acc. Chem. Res.* **2003**, *36*, 255−263.
(73) Rodriguez, J. A.; Kim, J. Y.; Hanson, J. C.; Pérez, M.; Frenkel, A. I. *Catal. Lett.* **2003**, *85*, 247−254.

DOI: 10.1021/jacs.7b11654
J. Am. Chem. Soc. 2018, 140, 1824−1833